Materials & Design 254 (2025) 114044

Contents lists available at ScienceDirect

Materials & Design

journal homepage: www.elsevier.com/locate/matdes

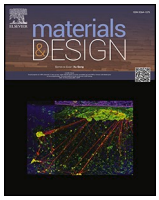

A statistical study on factors influencing piezoelectric properties of upside-down composites towards machine learning-driven development for recycling

Sivagnana Sundaram Anandakrishnan [a,b], Suhas Yadav [a], Mohadeseh Tabeshfar [a,b], Mikko Nelo [a,b], Jani Peräntie [a], Yang Bai [a,*]

[a] Microelectronics Research Unit, Faculty of Information Technology and Electrical Engineering, University of Oulu, Oulu FI-90570, Finland
[b] Infotech Oulu, Oulu FI-90570, Finland

ARTICLE INFO

Keywords:
Sustainable electronics
Composite modelling
High-throughput manufacturing
Lichteneker model
Yamada model

ABSTRACT

Using upside-down composites to recycle retired/discarded piezoceramics and then give them a second life in sensor applications paves the way towards sustainable production of piezoelectric materials. However, the piezoelectric properties of the recycled materials need to be significantly improved. The advancement of recycled materials should benefit from the recently developed AI-assisted methods, in order to minimize overconsumption of resources during the experimental trial and error. Previous works have identified obstacles to developing reliable models that can provide a systematic understanding of the contributors to the properties of the recycled materials. This work aims to overcome such obstacles by appropriately changing the fitting constants so that the models coincide with each experimental datapoint. These constants include descriptors of the microgeometry, size and orientation of the fillers, and the extent of polarization in the composites. By analyzing the variation of these constants between the datapoints, a clear perspective of the contributors to the properties of the recycled materials is established. This multi-variable approach is also extended to different fabrication techniques. The approach lays down a foundation for scaling up the optimization of the recycled materials by providing training and/or testing datasets for possible machine learning algorithms via potential high-throughput manufacturing routes.

1. Introduction

Piezoelectric ceramics (piezoceramics) are widely known for their excellent electromechanical coupling capability without the need for external voltage sources or moving parts [1]. This capability has been exploited in components crucial to modern electronics [1–4], earning the piezoelectrics industry a market worthy of billions of dollars [5,6]. Nowadays, the majority of piezoceramics are still fabricated using the traditional solid-state method typically conducted at temperatures above 1000 °C, which is essential for inducing the desired piezoelectric properties [7]. Even though the cold-sintering method has been invented for a while [8,9], in addition to its pressure-assisted synthesis and low-temperature densification, a high-temperature annealing treatment not far below typical sintering temperatures is still required to produce the needed crystallinity and thus functionality [10]. The necessity of such a high-temperature densification and grain growth step renders a large ecological footprint on the piezoelectrics industry [11].

Recycling of piezoelectrics is a viable remedy to reduce this footprint by extending the materials' lifespan. Research on recycling piezoelectric materials include the recycling of piezoelectric polymers and bio-piezoelectrics [12–16], the recycling of piezocatalysts [17–19], self-healing piezoelectrics [20,21], and the recycling of piezoceramics [11]. Compared to piezoceramics which is the focus of this work, piezoelectric polymers, bio-piezoelectrics and piezocatalysts generate much smaller ecological footprints owing to their lower fabrication temperatures. However, these materials generally show inferior piezoelectric properties and hence their applications are limited compared to those of piezoceramics. On the other hand, the self-healing research in piezoelectrics has been mostly exploratory in nature and the synthesis procedures tend to be complicated.

The simultaneous broad application range and large ecological footprint of piezoceramics bring the rationale of recycling piezoceramics

* Corresponding author.
E-mail address: yang.bai@oulu.fi (Y. Bai).

https://doi.org/10.1016/j.matdes.2025.114044
Received 15 January 2025; Received in revised form 21 April 2025; Accepted 2 May 2025
Available online 3 May 2025

through the upside-down composite method. The upside-down composites are made of crushed piezoceramics which can be fetched from old, worn-out, or rejected piezoelectric devices. The upside-down compositing method enables the recycling to be carried out at ultra-low temperatures (e.g., <350 °C) [11]. Known for their high filler volume fractions, which subscribes to the term "upside-down", the composites have displayed a competitive piezoelectric voltage coefficient (g [22], a figure of merit for piezoelectric sensors), with an energy budget of fabrication that is two orders of magnitude lower [23], compared to conventionally sintered piezoceramic counterparts.

Recent efforts on scaling up the recycling method as well as on improving the piezoelectric properties of the recycled piezoceramics [24] have inferred through experiments and modelling that the disparate permittivity between the filler and binder lead to low d (piezoelectric charge coefficient) values. The inherent mechanism is attributed to the lack of charge mobility in the binder that increases the charge relaxation time in it. Here, the charge relaxation time is the time taken for the injected charges in the binder from the poling electric field to dissipate to other portions of the composite until a specified percentage of the initial magnitude is reached [25]. This disrupts the electric field path in the composite by forcing most of the electric field to concentrate on the vicinity of the active filler phase at lower magnitudes [26–28]. The consequence is an increase in the coercive field possibly beyond the breakdown field of the composite so that obtaining a fully poled state becomes impractical [29].

Notwithstanding the low d values, the advantage of upside-down composites over monolithic piezoceramics is their ability to tailor for diverse end user requirements [30]. This ability stems from the structure of the composite itself consisting of two or more heterogeneous materials with different functional and structural properties, volume fractions, and interconnectivity [31]. For instance, upside-down composites are mechanically stiff owing to their high and changeable filler volume fractions [23,32].

Recycled piezoceramics may contain multiple types of filler sources with various properties. Therefore, being able to predict the composite properties fabricated from specific as well as mixed sources via modelling will stimulate the development of the recycling method. Previous works [24] have suggested that a combination of the Lichteneker and Yamada models could be suitable for predicting dielectric and piezoelectric properties of upside-down composites, especially for high filler volume fractions. However, the models deviated significantly from the experimental data for lower filler volume fractions. The pressure-assisted fabrication method at elevated temperatures which triggered the loss of binder that resulted in a change away from the designed volume fractions, rather than the models themselves, is to be blamed. Nevertheless, such a blame would not help to excuse the attempt to bridge the knowledge gap between upside-down composites with low and high filler volume fractions. Alternative approaches must be found.

Accelerated material design and development utilizing the high-throughput methodology is increasingly popular in modern piezoelectrics research. Most cutting-edge AI-driven material discoveries are directed towards predicting new piezoelectric ceramic compounds which could show advantageous properties that have not been explored in experiments. These discoveries typically employ first-principles density functional theory calculations [33–36], machine learning (ML) algorithms [37–40], or a combination of both [41] to avoid unnecessary experimental trials. Similar research has also been carried out for optimizing the properties of piezoelectric composites. For instance, phase field modelling, ML, and artificial neural networks have been used separately or combined to predict and optimize properties such as energy density, breakdown strengths, and electrical properties in piezoelectric composites [42–46].

Most of these material discovery works are focused on developing the models prior to the experimental validation, i.e., via the so-called "top-down" approach. Only a limited number of research [11,47] have devoted towards developing the models from data fed by experiments using a "bottom-up" approach. The bottom-up approach quantifies the intricate relationships present between the experimental conditions of fabrication and the physical properties of the composite samples, such as the correlation between their microstructure and functional properties. Therefore, providing a high-throughput research path for upside-down composites via a bottom-up approach to predict properties of the recycled piezoceramics from various sources and fabrication techniques will be tremendously beneficial.

For this reason, in this work we focus on interpreting the constants (k, n and α) used to fit the models to the experimental data, which provide a perspective on the microstructure (k and n) and the extent of polarization (α) of upside-down composites. Potential deviations of experimental data from the models can then be interpreted as changes in these constants due to certain change in the experimental conditions, for instance, the fabrication conditions and the properties of fillers and binders [48].

In this work, experimental d and permittivity datapoints derived from corresponding samples are assigned a set of the above-mentioned constants. We rationalize the trends in the values of these constants by using them as unconventional models to describe the changing inputs, including filler volume fraction and filler relative permittivity [29]. This approach is able to quantify the relationships among the fabrication technique, composite properties, filler characteristics, microstructure, and polarization states within each sample even if the model itself might not be applicable to the specific composite (i.e., suitable for training ML algorithms).

The datasets of the fitting parameters obtained in this work can then contribute as the input parameters to possible testifying of future high-throughput methods supported by ML algorithms for accelerated material design and development that could provide valuable insights into predicting the output given a set of input conditions [11,49,50], regardless of whether or not a universal model for upside-down composites can be derived.

2. Results and discussion

2.1. Description of initial datasets

Data associated with this work are openly available and can be accessed via the provided DOI link [51].

We extracted experimental data from literature for some major upside-down composites, as well as for two different types of piezoelectric composites that researchers frequently cite in modelling studies: dielectrophoretically (DEP) structured piezocomposites [52] and porous piezoceramics [53]. As has been discussed in previous works [24], the upside-down composite method is used to prepare ceramic-ceramic composites with high filler volume fractions (>75 vol%). The process employs a pressure-assisted densification procedure with a suitable binder phase at room temperature or at mildly elevated temperatures [54,55].

Briefly, the DEP structuring method is a technique used to transform a traditional 0–3 connected piezocomposite consisting of fillers randomly dispersed in a continuous binder to a quasi-1–3 connected structure by reorienting the fillers under an alternating current (AC) electric field. Typically, the transformation of the microstructure imbues the composite with more favorable functional properties [52]. In porous piezoceramics, porosity filled by air or other substances is intentionally introduced. Electrically, the air or material filling the pores acts analogously to a binder in upside-down or conventional composites and thus helps to significantly improve the g and $d{\cdot}g$ (a figure of merit for piezoelectric energy harvesting) [29].

Table 1 summarizes the information of experimental datasets used for the modelling in this work, including fabrication methods, fillers and binders, features of the samples, and input parameters. In the table, PT 1 and PT 2 were ceramics sintered in laboratory from commercial soft-type $Pb(Zr,Ti)O_3$ ceramic powders, PZ29 and APC-855 purchased from

Table 1
Summary of information of initial datasets used for the modelling in this work.

Fabrication method	Filler	Binder	Feature	Input parameter	Reference
Upside-down composites	PT 1, PT 2, PT 3, BT 1, BT 2, BT 3	(PTMA)$CdCl_3$	Fillers with similar d_{33} but distinctive permittivity	Filler permittivity	[24]
	PZ29	(PTMA)$CdBr_{1.5}Cl_{1.5}$	Varying filler volume fractions	Filler volume fraction	[22]
	PZ29	TiO_x	Various fabrication temperatures	Fabrication temperature	[56]
	$SrTiO_3$	$LiMoO_4$	Fillers with different modalities	Filler particle size/multi-modality	[57]
DEP structuring	PZ26, PZ27, PZT5A4, PZT507	Epoxy	Similar types of fillers but with varying permittivity and d_{33}	Filler volume fraction	[28]
	PZT5A	Epoxy	Different magnitudes of DEP structuring fields	Filler volume fraction	[58]
	(K, Na, Li)NbO_3	PDMS	Fibrous fillers	Filler volume fraction	[59]
Porous ceramics	BCZT	Air	Randomly distributed pores	Filler volume fraction	[60]
	BCZT	Air, Epoxy, PDMS	Parallel aligned pores	Filler volume fraction	[61]
	BCZT	Air, PDMS	Parallel aligned pores; Assembly of composite with pillar-base morphology	Filler volume fraction	[62]
	$BaTiO_3$	Epoxy	Randomly distributed and aligned pores; Selective alignments	Filler volume fraction	[63]
	PZT	Air	Aligned pores; Selective alignments	Filler volume fraction	[29]

Meggit A/S, Denmark and American Piezo International Ltd., USA, respectively. PT 3, BT 1, BT 2 and BT 3 were $67Pb(Mg_{1/3}Nb_{2/3})O_3$-$33PbTiO_3$, $(Ba_{0.80\pm0.02}Ca_{0.14\pm0.005})(Ti_{0.90\pm0.005}Zr_{0.10\pm0.005})O_{2.94\pm0.02}$, $(Ba_{0.95\pm0.01})(Ti_{0.94\pm0.005}Sn_{0.06\pm0.005})O_{2.95\pm0.01}$ and $(Ba_{0.79\pm0.01}Ca_{0.14\pm0.005})(Ti_{0.88\pm0.005}Zr_{0.12\pm0.005})O_{2.94\pm0.02}$ ceramics made in laboratory, respectively. Like PZ29, PZ26, PZ27, PZT5A4, PZT507, PZT5A and PZT were also $Pb(Zr,Ti)O_3$-based compounds processed in laboratory from corresponding commercial ceramic powders. The rest of the fillers in Table 1 were all made in laboratory, where BCZT represents compositions of $(Ba,Ca)(Zr,Ti)O_3$. (PTMA)$CdCl_3$ and (PTMA)$CdBr_{1.5}Cl_{1.5}$ were made in laboratory, while the rest of binders were all commercial products, where PDMS represents polydimethylsiloxane.

2.2. Upside-down composites

Fig. 1 plots the average values of the fitting parameters, $k_{average}$ and $\alpha_{average}$, as a function of different input parameters for upside-down composites. It can be noticed that almost all upside–down composite samples obtained negative $k_{average}$ values. This is because the pressure–based densification method squeezed a part of the binder solution which formed the transport phase out of the sides of the samples. This in turn aligned the fillers partially into series chain links, i.e., the connections between filler particles were more in perpendicular to the applied electric field direction during permittivity measurement or poling. Clear evidence is shown in Fig. 1b, where the $k_{average}$ approached 0 when the filler volume fraction (φ_f) decreased to approximately 0.4. This was a sign of the increased number of filler-binder interfaces being present in the composites as the φ_f decreased, which competed the overarching effect of the flow of the binder under pressure and thus effectively suppressed the series linked chains among the fillers.

The change of microgeometry also explains the much smaller $k_{average}$ for the Pb-free (BT 1-C, BT 2-C and BT 3-C) than for the Pb-based (PT 1-C, PT 2-C and PT 3-C) samples (Fig. 1a), as the binder volume fraction was larger for the latter. While constant negative $k_{average}$ values were observed amongst the Pb-based or the Pb-free samples, the PT 1-C had a slightly larger $k_{average}$, which is possibly attributed to two reasons: (1) A smaller mismatch between the relative permittivity of the PT 1 filler and the (PTMA)$CdCl_3$ binder, easing the surpassing of the percolation threshold [25,64] of the electric field permeation in the fillers. Here, the percolation threshold is the minimum filler volume fraction or relative permittivity mismatch between the filler and binder such that there is a creation of an interconnected pathway for the electric field to permeate from one electrode to another. (2) A higher T_C (Curie temperature) of the PT 1 filler [65] than those of the PT 2[66] and PT 3[67] fillers, inducing lower residual stress in the filler-binder interfaces upon cooling after fabrication [24].

The $k_{average}$ also increased with the fabrication temperature until 300 °C and then reached a plateau (Fig. 1c). The increase was attributed to the improving crystallization of the TiO_x binder, where the volume of crystallized binder became larger and thus less flowable. Therefore, the chance of binder being squeezed out during fabrication reduced, restricting the above-mentioned series linked chains among fillers. The plateau hence implied that the binder could not be further crystallized at 300 °C and above.

In addition, the $k_{average}$ increased with the increase of filler particle size (Fig. 1d). Fillers dispersed under mixed modal configurations with the majority being of larger size (MM2) seemed to show an even larger $k_{average}$. The larger $k_{average}$ for larger particle sizes was due to the lower surface energy [8] which decreased the probability of wetting by the binder and thus, resulted in less formation of series linked chains under pressure. In other words, the larger fillers were less easily pushed towards a series connection. The mixed modal configurations resulted in smaller fillers getting incorporated between the voids of larger fillers. This even further hindered the wetting compared to the unimodally distributed fillers.

The $\alpha_{average}$ values for the Pb-based (0.5–0.6) were generally higher than for the Pb-free (0.4–0.5) samples (Fig. 1e). This difference, again, was caused by the higher binder volume fraction in the Pb-based than in the Pb-free samples. The binder between the fillers acted as a crystalline bridge for the penetration of the electric field. This phenomenon can be further confirmed in Fig. 1f and g, where lower filler volume fractions induced larger $\alpha_{average}$ due to the presence of more crystalline bridges and, while most of the binders were well crystallized at higher temperatures, the $\alpha_{average}$ remained relatively constant.

However, the BT 3-C was found as an outlier with an $\alpha_{average}$ larger than 0.6. This was believed to be due to the BT 3 filler having a relative permittivity value (≈3400 at 1 kHz) far higher than that of the (PTMA)$CdCl_3$ binder, leading to the electric field concentration on the binder being so large that the dielectric breakdown strength of the binder could have been partially crossed and thus creating a conductive path which could have relatively evened the electric field distribution between the filler and binder.

The probable dielectric breakdown was evident from the increased difficulty of poling pellets made from hot-pressed, pure polycrystalline

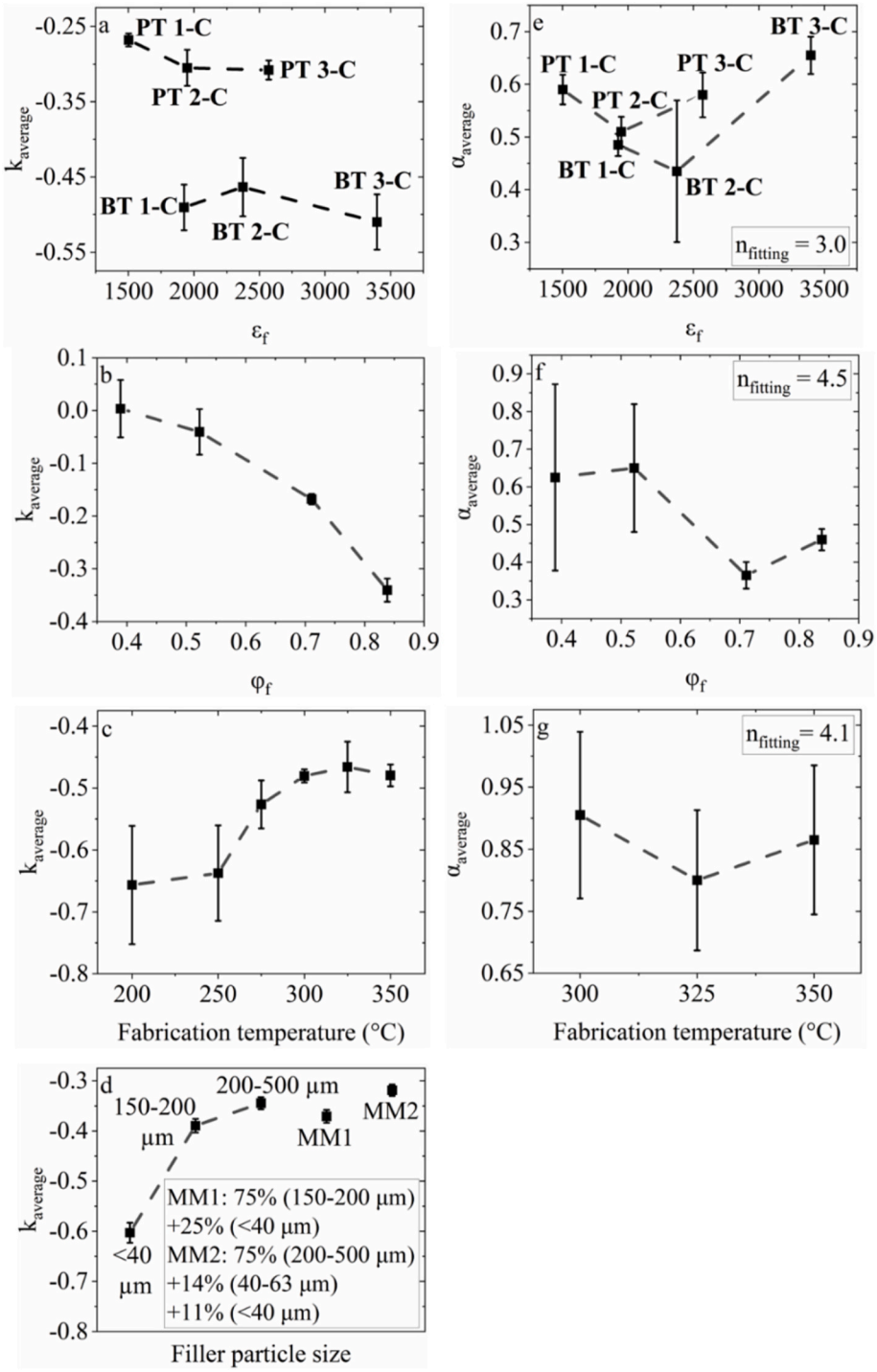

Fig. 1. Dependence of (a)-(d) $k_{average}$ and (e)-(g) $\alpha_{average}$ on (a)(e) filler relative permittivity (ε_f), (b)(f) φ_f, (c)(g) fabrication temperature and (d) filler particle size for the experimental data obtained from upside-down composites of (a)(e) samples with (PTMA)$CdCl_3$ as the binder and PT 1, PT 2, PT 3, BT 1, BT 2, BT 3 as the fillers [24], (b)(f) PZ29–(PTMA)$CdBr_{1.5}Cl_{1.5}$ [22], (c)(g) PZ29-TiO_x [56], and (d) $SrTiO_3$-$LiMoO_4$ [57].

(PTMA)$CdCl_3$ under the same conditions [22]. In this case, the broken parts of the (PTMA)$CdCl_3$ locally increased the dielectric loss [22,68]. This loss made applying a high electric field on a pure (PTMA)$CdCl_3$ pellet difficult but, on the other hand, paved a way to connecting electric fields between particles in composites.

It can be noticed that many upside-down composites showed large deviations of the $\alpha_{average}$. This was caused by large sample-to-sample variations, especially at lower filler volume fractions and at higher fabrication temperatures. Because (1) the crystallized interfaces when a higher volume of binder was involved or (2) the microcracks in the binders due to the rapid increase in elastic stiffness during crystallization tended to be more randomly distributed, the pathing of the applied electric field could be disrupted in a more unpredictable manner. The microstructural randomness was visible in the field emission scanning electron microscopy (FESEM) micrographs and the corresponding energy dispersive X-ray spectroscopy (EDS) maps of relevant works [22,56].

Despite the deviations, the samples in Fig. 1g showed much higher $\alpha_{average}$ of over 0.8. This is unambiguously a result of the optimization of poling conditions where the poling was performed at an elevated

temperature of 100 °C and for a longer period of 1 h compared to the room temperature and 10 min implemented for samples in Fig. 1e and f.

2.3. DEP structured composites

Fig. 2 shows the same types of data as those of Fig. 1 for DEP structured composites but with the filler volume fraction as the sole input parameter. Note that the filler volume fractions in Fig. 2 nicely extended below 0.4, the lower limit in Fig. 1b. The data validated many observations from the upside-down composites. For instance, for all the composites the $k_{average}$ generally decreased with the increasing φ_f (Fig. 2a-c). This indicates that even though the fillers were aligned, the relatively larger extent of series connectivity with a higher φ_f, which had been valid in upside-down composites, was also valid in DEP structured composites.

It is also confirmed that, within certain range of filler permittivity, similar $k_{average}$ values would be obtained. For the same φ_f, $k_{average}$ of PZ26-Epoxy approximated those of PZ27–Epoxy and PZT5A4-Epoxy (Fig. 2a) while the relative permittivity of PZ26 (1300) was much smaller than those of PZ27 (1800) and PZT5A4 (1850). However, PZT507 possessed a relative permittivity (4400) that was even much larger than that of the BT 3 (3400, Fig. 1a). This was believed to have caused the smaller $k_{average}$ for the PZT507-Epoxy samples.

These observations imply that, like in the upside-down composites, there was also a biasing effect in the DEP structured composites owing to the dielectric mismatch between the filler and binder. In theory, this effect should be absent in DEP structured composites because during fabrication, the uncured epoxy matrix was conductive and would more effectively distribute the electric field on the fillers. Therefore, it was inferred that the decrease in the $k_{average}$ was due to an inherent decrease in the composite permittivity rather than a change in the microgeometry.

The biasing effect of the binder on the electric field permeation in the composite was likely to reduce when the φ_f increased, as evidenced by the narrowing gap between the $k_{average}$ of the PZT507-Epoxy samples and those of the rest when the φ_f was approaching 0.4 (Fig. 2a). This fact suggests that due to the different fabrication techniques where the DEP structuring tended to induce a parallel connectivity while the upside-down composites tended to induce a series connectivity among the fillers, the upside-down compositing technique might possess an advantage for higher filler loading where the wetting of the fillers by the binder could be more efficient under the assisting pressures than the pressure-less method used in the DEP structuring technique.

Fig. 2b and c collaboratively demonstrate the correlation between the composite's microgeometry and $k_{average}$ value. For the same φ_f, $k_{average}$ increased from a random filler orientation to the case being aligned under 0.1 kV mm^{-1} and then further increased under 1 kV mm^{-1}, due to a larger number of fillers getting aligned in a parallel connection as the structuring electric field increased (Fig. 2b). An extreme case was that with fillers in a fiber shape, the $k_{average}$ drastically increased even for very low filler volume fractions (<0.08, Fig. 2c). This was clearly attributed to the fibers being able to form a much better parallel alignment due to their high aspect ratios. The large $k_{average}$ was also resulted from the lower dielectric mismatch between the KNLN fibers (≈360) and the PDMS binder (≈3).

The effect of filler-binder interfaces on $\alpha_{average}$ observed in the upside-down composites was also validated by the evidence of the decreasing $\alpha_{average}$ values with the increase of filler volume fractions (Fig. 2d–f), which was accompanied by the reduction in the number of filler-binder interfaces due to a weakened wetting result of the fillers by the binders. Instead, the interfaces were more likely occupied by voids, leading to a decrease in the poling efficiency due to the lower relative permittivity in the voids.

When the φ_f decreased, $\alpha_{average}$ between the PZ26-Epoxy composite and the rest of the composites (Fig. 2d) became more different, with the smallest gap of approximately 0.2 (i.e., $\alpha_{average}$ varying from 0.1 to 0.3) appearing at the φ_f of 0.4. For the similar Pb-based fillers, the upside-down composites only showed a gap of 0.1 (i.e., $\alpha_{average}$ varying from 0.5 to 0.6, Fig. 1e). The low permittivity mismatch between the PZ26 filler and epoxy enabled a more efficient permeation path for the poling electric field through the filler, while the PZ27, PZT5A4 and PZT507 fillers seemed to reach a saturation. By excluding the PZ26–Epoxy samples and only considering the mid-range filler relative permittivity, e.g., from PT 1 to PT 3 for 1500–2600 (Fig. 1e) and from PZ27 to PZT5A4 for 1800–1900 (Fig. 2d), the $\alpha_{average}$ values remained relatively constant within each category.

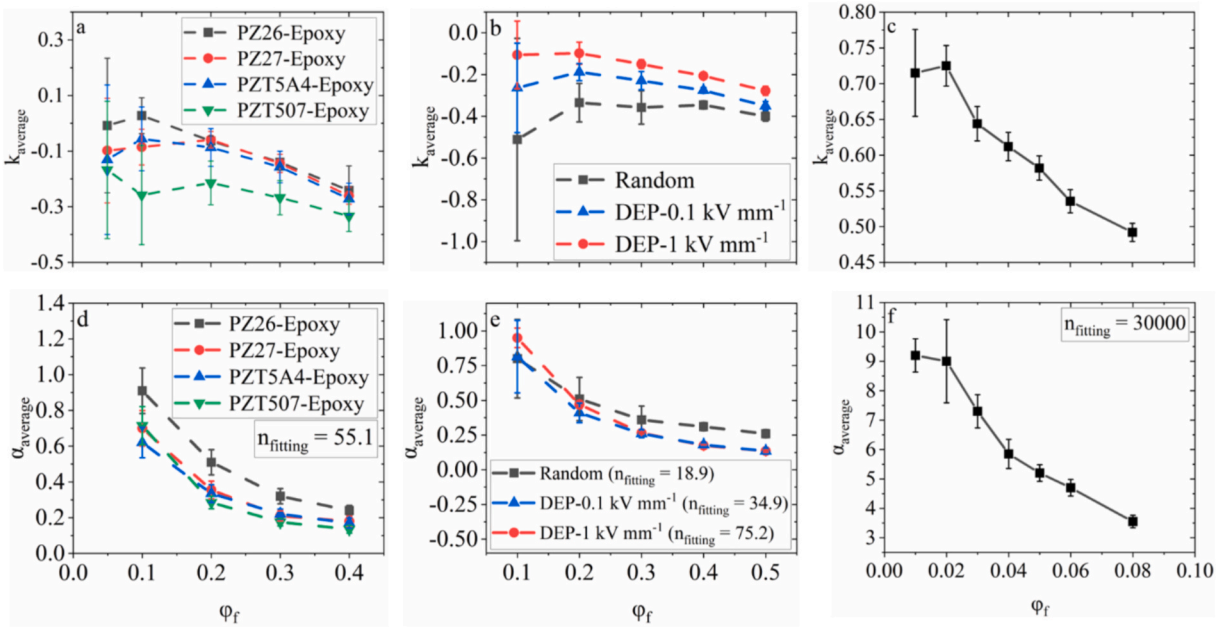

Fig. 2. Dependence of (a)-(c) $k_{average}$ and (d)-(f) $\alpha_{average}$ on φ_f for the experimental data obtained from DEP structured composites of (a)(d) samples with epoxy as the binder and PZ26, PZ27, PZT5A4 and PZT507 as the fillers [28], (b)(e) PZT5A-epoxy samples structured under different electric fields [58], and (c)(f) (K, Na, Li)NbO_3-PDMS samples [59].

According to the situation for the BT 3-C composite (Fig. 1e), the PZT507-Epoxy composite should have also experienced an increase in the $\alpha_{average}$ owing to a possible dielectric breakdown of the binder caused by the ultra-large relative permittivity of the PZT507 filler. However, no such increase was seen, which can be attributed to the larger breakdown strength of the epoxy than that of the (PTMA)$CdCl_3$ [69].

Surprisingly, the DEP structuring did not advantage the poling efficiency. As can be seen in Fig. 2e, the $\alpha_{average}$ of the structured composites was only higher at very low filler volume fractions. At higher filler volume fractions, the $\alpha_{average}$ of random composites surpassed those of the structured counterparts. This was because the random composites had roughly equal amount of filler-binder interfaces parallel with and perpendicular to the applied field, enabling a less disrupted electric field pathing in these composites compared to the structured ones. Indeed, the d_{33} of random composites showed a constant increasing trend with the increase of filler volume fractions while the structured composites saturated over filler volume fractions of higher than 0.4 [32,58].

The models in this work also successfully reflected the microstructure with steadily increasing $n_{fitting}$ values from random composites to composites with DEP structuring performed at 0.1 kV mm^{-1} and then to those at 1 kV mm^{-1} (Fig. 2e). As the level of the DEP structuring increased, a larger number of filler chains aligned in parallel with the electric field were formed with an increasing tendency towards the microstructure resembling the 1–3 composites.

Notably, even the random composite without any structuring procedure gave a large $n_{fitting}$ value. As the composite was poled during the curing of the epoxy binder, which was semi-viscous, it was likely that even the DC poling electric field caused a mild filler chain formation. This could be convinced when viewing the consistently greater experimental data than the modelling data for d_{33}[58] of the random composites at all filler volume fractions.

Nevertheless, it is easily noticed even the smallest $n_{fitting}$ value (18.9) in Fig. 2d-f was unbelievably large, pointing to unrealistic aspect ratios of the filler particles [28]. This was a consequence of using the Yamada model which was inapplicable for determining the d_{33} of the DEP structured composites. Eq. (1) shows the actual model for DEP structured composites in literature [52].

$$d_{33c} = \frac{(1+R)^2 \varepsilon_b \varphi_f Y_{33f} d_{33f}}{(\varepsilon_f + R\varepsilon_b)[(1+R\varphi_f)Y_{33f} + (1-\varphi_f)RY_{33b}]} \quad (1)$$

In Eq. (1), the constant R is calculated as the ratio of the filler particle size to the interparticle distance within the composite. R describes a new type of electrical interaction occurring in DEP structured composites, i.e. the relative particle sizes and their distance between one another which affects the electric field pathing in the fillers. Y_{33} refers to the longitudinal elastic modulus of the respective phase measured in parallel with the direction of the applied electric field. Y_{33} describes a new type of mechanical interaction, i.e., the relative distribution of mechanical input load between the fillers and binders during the d_{33} measurement. The subscripts denote the phases, i.e., c – composite, f – filler, and b – binder. As can be seen, the inapplicability of the Yamada model for DEP structured composites was a result of the lack of necessary descriptive constants.

In this work, the $n_{fitting}$ values, despite being unrealistic, can still be used for distinguishing between the fabrication techniques and the microstructure within each technique due to the uniqueness of $n_{fitting}$ values for each type of fabrication as well as their discrepancy for different microstructures. For instance, ordinary $n_{fitting}$ values (Fig. 1e–g) clearly define the upside-down composites and extremely large $n_{fitting}$ values (Fig. 2f) unambiguously tell apart DEP structuring with fibrous and non-fibrous fillers. Various, moderately large $n_{fitting}$ values indicate the structuring level of non-fibrous fillers (Fig. 2d, e).

Different from the non-fibrous counterparts, the DEP structured composites made from fibrous fillers also gave unrealistically large $\alpha_{average}$ (3–9, Fig. 2f) as an extreme consequence of missing R and Y_{33} in the model used in this work. It is deduced here that while unrealistic $n_{fitting}$ values will be useful in potential ML algorithms, unrealistic $\alpha_{average}$ values may exclude composites with fibrous fillers, especially those with extremely low filler volume fractions (e.g., <0.1), from the scope of this study. After all, making upside-down composites with extremely low filler contents would be either unrealistic or meaningless.

2.4. Porous ceramics

Taking advantage of the above learning outcome, in an analogous way, Fig. 3 studies the porous composites with both varying filler types and contents as well as with diverse microstructural alignments, which resemble the scenarios for both the upside-down and DEP structured composites. Although the situation became much more complex, conclusions made above are still valid. For instance, the same filler microgeometry would induce similar $k_{average}$. For the same randomly distributed pores or the same binder alignments, constant $k_{average}$ values were obtained within certain φ_f ranges when considering the deviations (Fig. 3a–e).

It can be noticed that deviations of some $k_{average}$ and $\alpha_{average}$ values were abnormally large. This is because the actual experimental deviations of relative permittivity and d_{33} for each datapoint were not provided in the cited works. In order to realistically reflect possible sample-to-sample variations, a deviation of ±10 % was assigned to the pristine experimental data for the calculation of $k_{average}$ and $\alpha_{average}$. This assigned deviation is considered an upper/bottom limit of experiments to be able to believe the reported data, and hence the magnitude is proportional to the absolute values of relative permittivity and d_{33}. The actual deviation between samples was expected to be smaller than the calculated values.

The increasing $k_{average}$ at $\varphi_f > 0.82$ (Fig. 3a) was attributed to the large relative permittivity seen in these composites, which was a consequence of the three-dimensional connectivity in the filler (larger parallel connectivity) that effectively retained a larger portion of the electrical properties. As evidenced in the microstructure [60], connected pores formed a pore-wall network (open pores) and were predominantly present at low φ_f, which then gradually transformed into isolated, closed pores at high φ_f. In other words, a quasi-2–2 connectivity was transformed to a 0–3 connectivity as φ_f increased. This indicates a drastically different morphology compared to the upside-down and DEP structured composites. The difference was also evident from the positive $k_{average}$ values for all the porous composites (Fig. 3a-e) comparing to the consistently (Fig. 1) and partially (Fig. 2) negative ones for the upside-down and DEP structured composites, respectively.

When the pores or binders were aligned in parallel with the direction of the applied electric field, the freeze casting process induced large $k_{average}$ values approaching 1 (Fig. 3b–e). However, the $k_{average}$ derived from the complex pillar-base arrangement (Fig. 3c) was lower than the ordinary freeze casting method (Fig. 3b). According to the schematics [62], the pillar and base had different orientations of the aligned channels for each phase, and the PDMS occupied a large portion between each pillar. As a result, the overall parallel alignment of the filler was reduced for the entire structure.

On the other hand, the considerably constant $k_{average}$ with varying φ_f revealed the advantage of the pillar-based freeze casting technique for highly precise production which could minimize series connections between adjacent ceramic planes.

The influence of binder alignment on $k_{average}$ is more clearly illustrated in Fig. 3d and e. The $k_{average}$ for a parallel alignment (C ∥ E) was always larger than those of no alignment or series connectivity (C ⊥ E). The angled alignment (C ∠ E) contributed a moderate $k_{average}$ in between [63]. Meanwhile, the ideal $k_{average} \approx 1$, $0 < k_{average} < 1$, and $k_{average} \approx 0$ were achieved for the C ∥ E, C ∠ E, and random composites, respectively. These results are in line with the theory.

However, the PZT-Air composites with series connectivity (C ⊥ E) had a constant value of $k_{average} \approx 0$ instead of the expected $k_{average} \approx -1$.

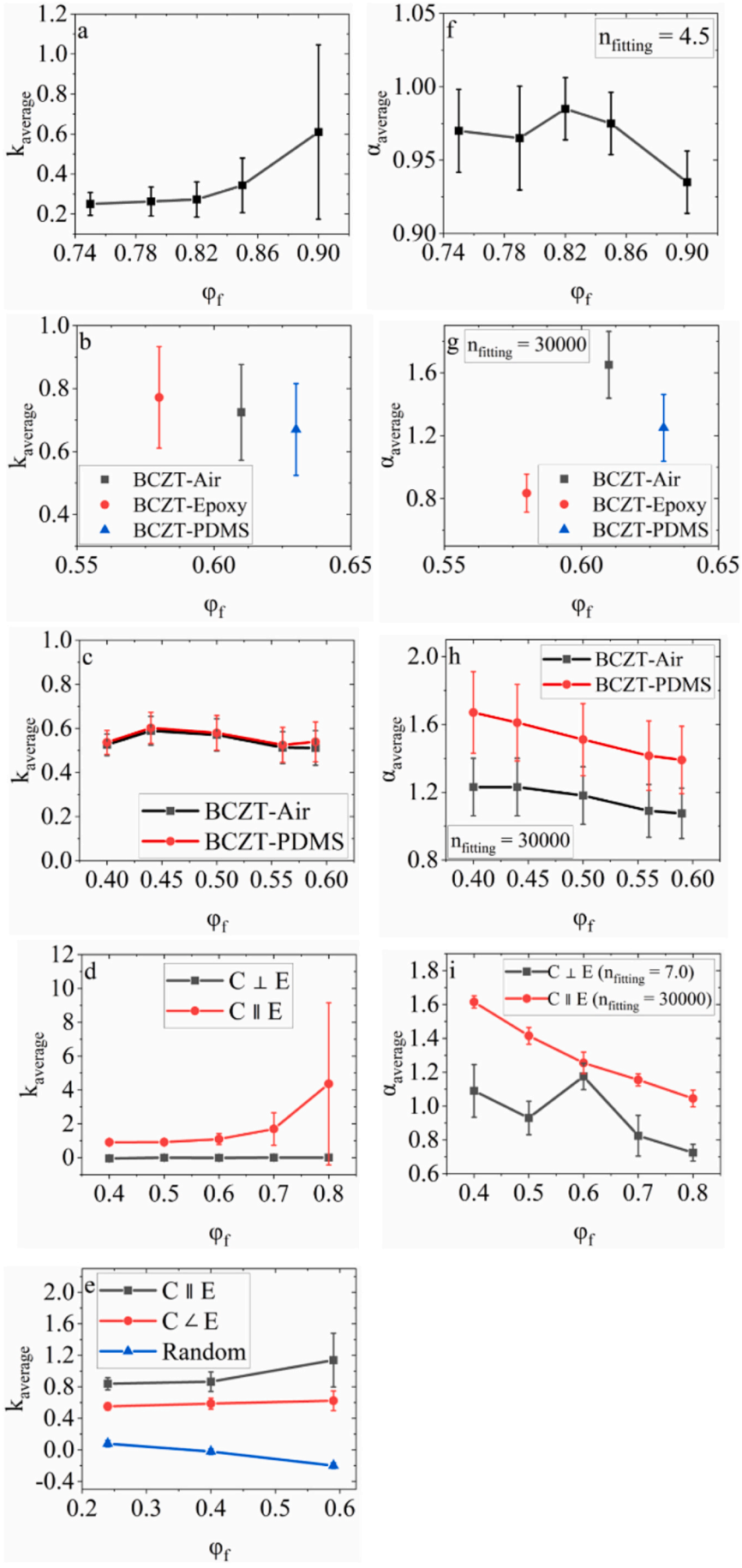

(caption on next page)

Fig. 3. Dependence of (a)-(e) $k_{average}$ and (f)-(i) $\alpha_{average}$ on φ_f calculated from experimental datasets of porous composites: (a)(f) BCZT-Air with randomly distributed pores [60], (b)(g) BCZT–Air, BCZT-Epoxy and BCZT–PDMS with parallel binder alignment [61], (c)(h) BCZT-Air and BCZT-PDMS with parallel binder alignment and pillar-base morphology [62], (d)(i) PZT-Air with different pore alignments [29], and (e) $BaTiO_3$-Epoxy with aligned and randomly distributed pores filled by epoxy [63].

This is an interesting phenomenon and could be due to the complete closure of some of the aligned pores by the ceramic walls during the cutting procedure. As these composites had a lower compressive strength compared to the C ∥ E composites along the cutting direction, complete closure of the pores was more likely to occur in this case as opposed to mild closures that would increase the connectivity in the perpendicular direction of the ceramic walls. This resulted in a slight parallel connectivity in these composites, rendering a higher $k_{average}$.

The above-mentioned attempt of using the $n_{fitting}$ values to distinguish fabrication techniques is nicely validated in Fig. 3f–i, where realistic $n_{fitting}$ values (<10) with $\alpha_{average}$ that stays very close to or slightly above 1 indicate the porous ceramics containing pores/binders with random distribution or series connectivity (Fig. 3f and i). This feature makes the porous ceramics with random pore/binder distribution almost identical to the upside-down composites (Fig. 1e–g), whilst a tendency of showing slightly higher $n_{fitting}$ or $\alpha_{average}$ could still be noticed on those of series connectivity if a wide range of φ_f was calculated (Fig. 3i).

Extremely high $n_{fitting}$ (e.g., 30000) paired with moderate $\alpha_{average}$ (e.g., <3) indicates the porous ceramics with parallel pore/binder connectivity (Fig. 3g–i), which makes a difference from the DEP structured composites with fibrous fillers constantly showing unrealistically large $\alpha_{average}$ (Fig. 2f). Certainly, composites with fibrous fillers could also be naturally recognized with their extremely low filler load.

The large $\alpha_{average}$ was indicative of the optimized poling conditions. However, the unrealistic $\alpha_{average}$ of larger than 1 was believed to be due to the different input mechanical loads taken by the respective phases in the composite during the d_{33} measurement caused by the alignment procedure, similar to the case of DEP composites as discussed above, which was not considered in the Yamada model adopted in this work. For the porous composites, the input mechanical load on the active ceramic phase can be quantified by the storage moduli (E') of the binder.

Eq. (2) and Eq. (3) express the models used for predicting the d_{33} of composites with parallel ($d_{33\text{-}C \parallel E}$) and perpendicular ($d_{33\text{-}C \perp E}$) pore/binder alignments, respectively, in a 2–2 type connectivity between the ceramic and binder phases [29].

$$d_{33-C\parallel E} = \frac{\varphi_f d_{33f}}{\varphi_f + (1-\varphi_f)(E'_b/E'_f)} \tag{2}$$

$$d_{33-C\perp E} = \frac{\varphi_f d_{33f}}{\varphi_f + (1-\varphi_f)(\varepsilon_f/\varepsilon_b)} \tag{3}$$

According to Eq. (2), the $d_{33\text{-}C \parallel E}$ is inversely proportional to the ratio of the storage moduli between the binder and ceramic phases, which clearly elaborates the observed trends of $\alpha_{average}$ (Fig. 3g). Epoxy has a large value of storage modulus ($E' \approx 2900$ MPa [70]) than those of air (0) and PDMS (1.72 MPa [71]). The larger the E' value, the more evenly distribution of input mechanical load among the phases during the d_{33} measurement. Therefore, the lower effective loading on the active ceramic phase in the BCZT-Epoxy composites yielded a lower d_{33} value and, despite the identical poling conditions, the BCZT-Epoxy composites obtained a lower $\alpha_{average}$ than those of the BCZT–PDMS and BCZT-Air counterparts.

On the contrary, according to Eq. (3), there are no parameters that relate the $d_{33\text{-}C \perp E}$ to any mechanical properties of the respective phases. As a result, the $\alpha_{average}$ values for the samples with a series connectivity were brought down to the realistic range below 1 from the unrealistic values for those with a parallel connectivity, both under the optimized poling conditions (Fig. 3i).

Based on what was learnt from the DEP structured composites, at φ_f beyond certain threshold the $\alpha_{average}$ would barely change anymore (Fig. 2d, e). However, the $\alpha_{average}$ showed much more obvious decreasing trends with the increase of φ_f in Fig. 3h, i. This could be attributed to the increasing probability of minor misalignments in the ceramic walls as filler volume fractions increased during the cutting procedure that was performed for aligning the phases in a particular direction. These minor misalignments were visible in the microstructure [29], which would have decreased the number of filler-binder interfaces and thus causing a disruption in the electric field pathing during poling.

The pillar-base morphology can have a major influence on $\alpha_{average}$. At higher φ_f, the injected binder might not have been able to completely penetrate through the pores because a larger capillary pressure was needed as the widths of the pores decreased. The pores that were left unfilled or partially filled with air resulted in a lower $\alpha_{average}$. Meanwhile, different from that in the conventional cylindrical samples with parallel alignments, the pillar–base configuration transferred the mechanical load applied to the composite during the d_{33} measurement to a bending load. Due to the low bending stiffness of the PDMS binder, a higher degree of bending deformation occurred in the BCZT–PDMS composites than in the BCZT-air ones. This enabled a larger load transfer to the active ceramic phase and consequently larger d_{33} and $\alpha_{average}$ values, resulting in the opposite trends in Fig. 3g and h. Here, analogous to the storage moduli in Eq. (2), a bending stiffness constant could be accounted in the Yamada model to avoid $\alpha_{average}$ values being larger than 1. However, such a constant cannot be validated yet since no analytical model predicting the piezoelectric properties of a composite with a pillar-base configuration has been reported.

2.5. Demonstration of a training dataset for possible ML algorithms

Tables S1–S3 in the Supplementary Material summarize the significant results obtained from the unconventional modelling approach conducted on the experimental datasets analyzed in this work. Table S4 then lists the dependent parameters for each fabrication technique that influence the dielectric and piezoelectric properties of the resulting composites.

Fig. 4 summarizes the n, α and k values obtained above. The most significant advantage of this method is that without considering the input parameters, a perspective on the distribution of the fitting parameters, each of which is unique to its corresponding fabrication technique and boundary conditions, can already be drawn.

The first layer of differentiation is identification through n values displayed in Fig. 4a. When an unrealistically large n value (> 10000) is detected, it can be instantly determined that the composite contains extremely high-level structuring, including the DEP structured composites with aligned fiber fillers, as well as parallel aligned and pillar-base assembled porous ceramics. When an unrealistic but moderate n value (10–100) is seen, DEP structured composites with no specific filler morphology can be exclusively identified. When the n value falls below 10 into the realistic range, the composite structure can be determined as random or series connected, including all upside-down composites, as well as porous ceramics with random and series connectivity.

The second layer takes advantage of the dependence of α on microgeometry (Fig. 4b and Tables S1–S3), despite α primarily depends on the poling conditions which are not influenced by the fabrication technique. This layer is particularly sensitive to fibrous fillers. For instance, the DEP structured composites that cannot be distinguished in the first layer easily possess unrealistically large α values (>2) and can thus be separated from highly structured porous ceramics which show α values floating around 1 (the realistic-unrealistic border).

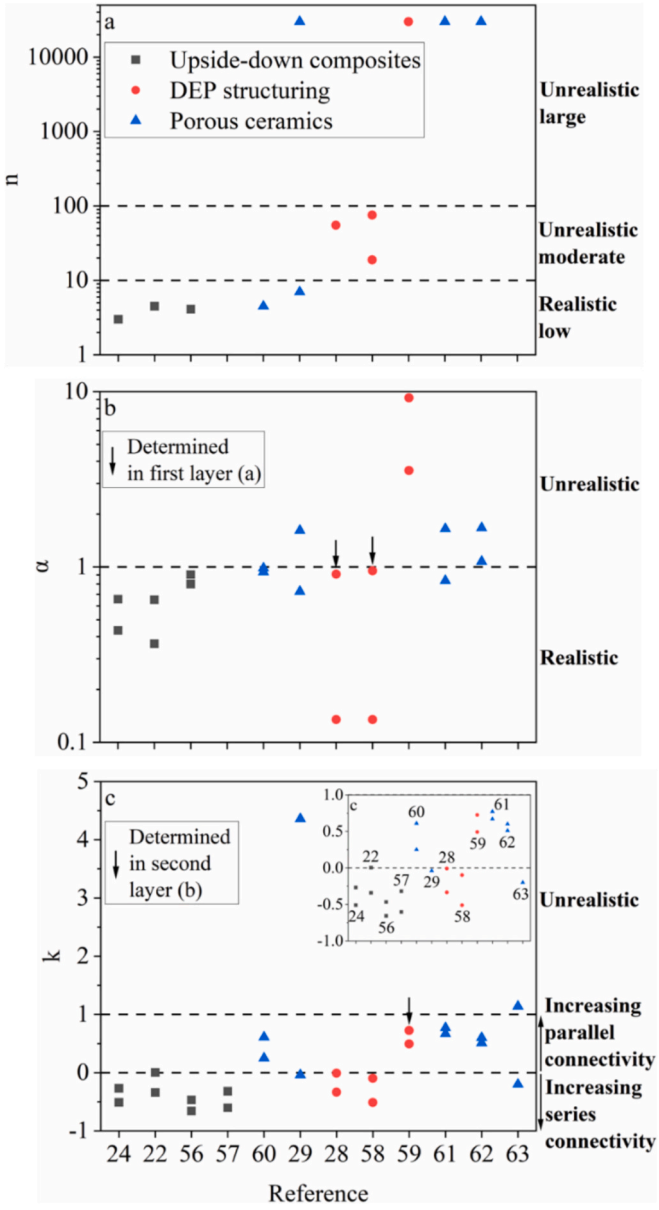

Fig. 4. (a) n, (b) α, and (c) k values obtained from all composites studied in this work.

The third layer can differentiate the rest of the datasets further via k, as displayed in Fig. 4c. Upside-down composites never reach a k value of above zero. On the contrary, random porous ceramics consistently yield above-zero k values, whilst porous ceramics with series connectivity show quasi-zero k values. A stark contrast is also noticed between the k values of parallel aligned porous ceramics (much larger than 1, in the unrealistic region) and porous ceramics with pillar–base assembly and dominant parallel connectivity (≈ 0.5, in the realistic region).

Therefore, it is not complicated to foresee that if a future ML algorithm can be fed with a sufficient amount of such training data containing the fitting parameters of n, α, and k, the nature of an unknown composite can be recognized by artificial intelligence and thus offer a simple yet effective strategy for fingerprints of each fabrication technique and filler/binder geometry, which can further stimulate the design and optimization of the resulting functionality of the composites. Potential material optimization routes are discussed in Section 2S in the Supplementary Material.

To substantiate our findings that the unconventional modelling methodology developed in this work can provide a suitable training dataset for ML algorithms, two additional experimental datasets [72,73] from some other upside-down composites were used as the testing datasets and were modelled using the same methodology. Section 3S in the Supplementary Material elaborates the testing data. Fig. S1 plots the $k_{average}$ and $\alpha_{average}$ as a function of different input parameters. Fig. S2 shows the range of k, n and α values obtained from the testing data which are then compared with those of the training data. Figs. S1 and S2 clearly indicate that the testing data possess the same fingerprint of the upside-down composite fabrication technique with what has been seen in Fig. 4: $n < 10$ and $\alpha < 1$ in the realistic regions, and $k < 0$ in the series connectivity region.

2.6. Applicability of ML algorithms

The unconventional methodology developed in this work is applicable to both regression (linear and logistic) and neural networks. Some example applications for predicting and improving the recycled piezoceramics are given as follows:

(1) Linear regression: A large amount of literature data of piezoelectric composite properties can be fed to the computer. The input variables may include the composition and properties of fillers and binders, the filler volume fraction, and the composite properties. For a new piezoceramic filler to be recycled, the results of the linear regression will suggest the favored fabrication technique and the corresponding required microstructure (filler particle shape and type of particle connectivity) and extent of poling based on the properties of the closest possible counterpart.
(2) Logistic regression: When multiple types of piezoceramics are to be recycled into a single material (e.g., due to the mixture of the source materials that cannot be easily separated), different weights may be assigned to the input variables. Conflicts could exist in practice. For example, filler A might prefer a series connectivity in upside-down composites to reach the best possible properties while filler B might need a parallel connectivity in DEP structured composites. When these two fillers are recycled simultaneously, results from the logistic regression may suggest which input variable is more important and then the best possible selection of fabrication technique, microstructure and poling can be achieved.
(3) Neural networks: In fact, Fig. 4 presents a very brief neural network with three layers. For a new piezoceramic filler to be recycled, we may want to prioritize the use of upside-down composites. The literature data then need to be screened through the layers to make sure the property estimation is indeed for the same upside-down compositing method rather than for other fabrication techniques. After the screening procedure, regression may be combined to help to further optimize the microstructure and poling, as described above.

3. Conclusions

The issue of significant and unpredictable deviations of experimental dielectric and piezoelectric data of upside-down composites at low filler contents from existing models have been found to hinder the potential high-throughput development for scaling up the recycling capability of piezoceramics using the upside-down composite method. This work has attempted to solve this issue by exploring an alternative methodology. Instead of adjusting the models incrementally, this work fits each experimental datapoint of permittivity and d_{33} with the modelling constants from the Lichtenecker and Yamada models, i.e., k and n which represent the microstructure and α which represents the extent of polarization, considering the deviations. The trends of these datapoints are analyzed with respect to changing input parameters such as the filler volume fraction and are then rationalized with anticipated origins as unconventional models.

Beside upside-down composites, this unconventional approach has also been extended to other piezoelectric composites fabricated via DEP structuring and porous ceramics. Departing from the conventional approach of fitting each individual composite into proper models containing adjusting constants, this work has successfully unified the viewpoints towards upside-down composites with other composites in terms of specific filler morphologies and alignment procedures. This unconventional approach provides multiple layers of taxonomical differentiation/classification that are suitable for the logic of ML algorithms comparing to calculation-based models.

Utilizing this datapoint-wise modelling approach, correlations between the fabrication technique, functional properties, input parameters, microstructure, and the extent of polarization within each sample are established. The combined trends of k, n and α obtained with respect to various input parameters serve as possible testing datasets for future ML algorithms in order to accelerate material development via high-throughput design. Upon rigorous training of such a possible algorithm, valuable insights into predicting composite properties selectively tailored towards a particular application based on desired, multi-modal filler(s) and binder(s) can be established. This will drastically reduce the need for time-consuming experimental studies and for calculation-based universal model development.

As a step towards developing a unified methodology for seamless prediction of functionality in any type of electronic composite, the taxonomical approach in this work combined with the recently demonstrated, tremendous capability of ML approach [74] in processing large datasets looks promising. Future work may introduce succeeding layers for differentiation using values including d_{33}, permittivity, and filler volume fraction. Such succeeding layers can be used to further identify datasets to a subtler extent, for instance, between BT-based and PZT–based compounds.

Recycling piezoceramics complies with necessary ethical considerations regarding environmental regulations [11]. A concrete next step can be investigating the simultaneous recycling of multiple piezoceramic fillers either due to the mixture of the source materials that cannot be easily separated or for the aim of tailoring/optimizing the properties of the recycled materials. Using the methods outlined in Section 2.6, a series of possibilities may be predefined, including the options for combinations of fillers and binders with specific conditions of the composite microstructure and poling states. A high-throughput experimental validation could then be carried out to assist in mixing the large number of options for fillers and binders. A multidimensional map illustrating the correlations among filler combination, binder selection, fabrication technique, microstructure, poling state, and composite properties can established, which serves as a guidebook or material pool for future recycled materials. In terms of the scalability, any simple hydraulic pressure apparatus with mild heating capabilities (e.g., 350 °C) present in typical industrial settings will suit the purpose.

4. Materials and methods

4.1. Modelling theory

In this work, the modelling of the experimental relative permittivity and d_{33} data were performed using the Lichteneker [75] and Yamada models [76] given by Eqs. (4) and (5), respectively. These models were chosen over other representative models owing to their applicability towards modelling upside-down composites as seen in previous work [24]. The screening procedure for the modelling approaches is described in Section 4S in the Supplementary Material. Figs. S3, S4 and Table S5 in the Supplementary Material compare the fitting results of different models. Using the Least-Squares method, the Lichteneker and Yamada models were determined to be the best solution for this work.

$$\varepsilon_c^k = \varepsilon_f^k \varphi_f + \varepsilon_b^k \varphi_b \tag{4}$$

$$d_{33c} = \frac{n\varphi_f \alpha \varepsilon_c d_{33f}}{n\varepsilon_c + \varepsilon_f - \varepsilon_c} \tag{5}$$

In Eqs. (4) and (5), subscripts c, b, and f refer to the composite, the binder phase, and the filler phase, respectively. ε corresponds to relative permittivity, φ corresponds to volume fraction of a phase in the composite, d_{33} refers to the longitudinal piezoelectric charge coefficient, n refers to a constant which is the inverse of the depolarization factor describing the shape anisotropy effects of the fillers, α refers to a constant that quantifies the poling efficiency of the composite, and k refers to a constant describing a specific microgeometry of the fillers in the composite.

The fitting constants of Eqs. (4) and (5) describe the microstructure and the extent of polarization, and they possess specific boundary conditions. The value of k is dictated by the Wiener boundary conditions ($-1 < k < 1$). $k = 1$ and $k = -1$ indicate fillers aligned in parallel with and perpendicular to, respectively, the direction of applied external electric fields during dielectric measurements and poling, i.e., parallel connection and series connection, respectively. $k = 0$ indicates fillers randomly distributed in the continuous binder, akin to a 0–3 connected composite.

The minimum value of $n = 3$ indicates a composite microstructure dispersed with spherical fillers with no orientational effects, while values of $n > 3$ indicate elongated fillers towards the direction of the applied external force during the d_{33} measurement. The maximum value $n = 10$ was a realistic limit on the value of n given from literature, as beyond this value an unrealistic aspect ratio for the fillers would be derived. α represents the poling efficiency of the composite with regards to a theoretical maximum, $\alpha = 1$, which is achieved under the optimum poling conditions including electric field, time, and temperature [48,77].

4.2. Modelling method

Different from the conventional modelling of piezoelectric composites where all datapoints in an experimental dataset are fitted by a specific model, this work utilized an unconventional modelling methodology to interpret the values of the fitting constants from each datapoint. The potential fitting errors and the limitations associated with using the conventional modelling technique for composites are demonstrated in Section 5S in the Supplementary Material.

The results shown in Fig. S5 and Table S6 in the Supplementary Material nicely demonstrate the limitations of the conventional modelling methodology where large errors are observed. In the case of the upside-down composites, the deviations were attributed to a change in the fabrication conditions where binder expulsion and evaporation, due to the applied pressure and elevated temperature, caused an unpredictable change in the φ_f. In the case of the other sets of data, the deviations were attributed to the inapplicability of the Lichteneker and Yamada models for these composites. The models were applicable only for biphasic composites consisting of isotropic fillers distributed in a homogenous binder with relatively high filler volume fractions with no specific alignments, as has been elaborated in Sections 2.3 and 2.4 above. In other words, the boundary conditions [75,78] in which the models were analytically derived differed from the boundary conditions generated during fabrication in the DEP structured composites and porous ceramics which have anisotropic fillers with specific alignments along with a different order of connectivity between the phases as well as lower filler volume fractions. The need for breaking these boundary conditions motivated the unconventional modelling approach explored in this work.

A detailed step-by-step workflow describing the entire modelling is elaborated in Section 6S in the Supplementary Material, where Fig. S6 shows a flowchart of the work procedures and Fig. S7 shows the results of the generated unconventional models from the identical experimental datasets considered for the conventional modelling approach (Section

5S in the Supplementary Material).

In brief, during the fitting procedure in this work, experimental data of relative permittivity and d_{33} were extracted from corresponding works and publications (see Table 1) and then fed into Eqs. (4) and (5) to calculate the k and α with an appropriately fitted n value ($n_{fitting}$). For those data where the experimental deviations were not provided, a ± 10 % deviation was assigned to each experimental relative permittivity and d_{33} datapoint. The average k and α, hereby designated as $k_{average}$ and $\alpha_{average}$, were plotted along with their deviations against the varying input parameters.

In particular, for the lowest filler volume fractions, the highest possible realistic α value (1 or close to 1) was firstly set, and then the appropriately fitted n value was found by matching the model with a certain datapoint. This n value was then applied to all similar datapoints, and then, in turn, an appropriate α was found. The extreme case was seen on the DEP structured composites with fibrous fillers, where the n reached a too high value whose further change would barely move the datapoint closer to the model. Here, the α value (by setting the maximum n value) became the primary factor that affects the fit of the model.

4.3. Composite fabrication techniques

The fabrication techniques for upside-down composites [8,22,23,54–57,79,80], DEP structured composites [25,26,28,58,59,81], and porous ceramics [29,82] are well documented in literature. Detailed descriptions of these techniques can be found in Section 1S in the Supplementary Material. Although the high-throughput material optimization routes for improving the functionality of the composites are beyond the scope of this study, recent research indeed have involved the use of fabrication techniques such as inkjet or 3D printing for upside-down composite fabrication [83,84] and porosity introduction [85]. These techniques can potentially be used for recycling piezoceramics in collaboration with the modelling method developed in this work.

The performance of the recycled piezoceramics in devices could be further predicted using AI and machine learning techniques for real-world applications [46,86–88]. For instance, the modified Jiles-Atherton model may be combined with neural networks to predict the performance of piezoelectric actuators made from the recycled materials [89].

CRediT authorship contribution statement

Sivagnana Sundaram Anandakrishnan: Writing – original draft, Visualization, Methodology, Investigation, Formal analysis, Data curation, Conceptualization. **Suhas Yadav:** Methodology, Conceptualization. **Mohadeseh Tabeshfar:** Investigation. **Mikko Nelo:** Writing – review & editing, Supervision. **Jani Peräntie:** Writing – review & editing, Supervision. **Yang Bai:** Writing – review & editing, Validation, Supervision, Resources, Project administration, Methodology, Funding acquisition, Conceptualization.

Funding

This research is funded by Infotech Oulu as a spearhead project and is co-funded by the European Union (ERC, UNIFY, 101039110). Views and opinions expressed are however those of the authors only and do not necessarily reflect those of the European Union or the European Research Council. Neither the European Union nor the granting authority can be held responsible for them.

Declaration of competing interest

The authors declare that they have no known competing financial interests or personal relationships that could have appeared to influence the work reported in this paper.

Acknowledgements

The authors acknowledge the Centre for Material Analysis, University of Oulu for providing necessary facilities and expertise for sample processing and measurements. The authors also acknowledge Prof. Heli Jantunen and Adj. Prof. Jari Juuti for insightful discussions related to the work, and Dr. Jaakko Palosaari and Mr. Vasilii Balanov for research assistance.

Appendix A. Supplementary data

Supplementary data to this article can be found online at https://doi.org/10.1016/j.matdes.2025.114044.

Data availability

The data that support the findings of this study are openly available in Faidata.fi Etsin at DOI: https://doi.org/10.23729/fd-4296899f-a945-3eb1-9a77-49baa24744af, reference number [51].

References

[1] Y. Bai, H. Jantunen, J. Juuti, Adv. Mater. 30 (2018) 34, https://doi.org/10.1002/adma.201707271.
[2] B.P. Abbott, R. Abbott, T.D. Abbott, V. Pecunia, S.R.P. Silva, J.D. Phillips, E. Artegiani, A. Romeo, S. Barth, F.R. Fan, W. Wu, P. Costa, J. Campo, J. Phys. Mater. 6 (2023) 4, https://doi.org/10.1088/2515-7639/acc550.
[3] H. Jaffe, J. Am. Ceram. Soc. 41 (11) (1958) 494, https://doi.org/10.1111/j.1151-2916.1958.tb12903.x.
[4] Y. Bai, Appl. Phys. Lett. 124 (2024) 11, https://doi.org/10.1063/5.0193134.
[5] J. Rödel, K.G. Webber, R. Dittmer, W. Jo, M. Kimura, D. Damjanovic, J. Eur. Ceram. Soc. 35 (6) (2015) 1659, https://doi.org/10.1016/j.jeurceramsoc.2014.12.013.
[6] K. Uchino, Sci. Technol. Adv. Mater. 16 (2015) 4, https://doi.org/10.1088/1468-6996/16/4/046001.
[7] A.J. Moulson, J.M. Herbert, Electroceramics:Materials, Applications, Properties, 2003, pp. 95–130.
[8] J. Guo, R. Floyd, S. Lowum, J.-P. Maria, T. Herisson de Beauvoir, J.-H. Seo, C. A. Randall, Annu. Rev. Mater. Res. 49 (2019) 275, https://doi.org/10.1146/annurev-matsci-070218-010041.
[9] J.P. Maria, X. Kang, R.D. Floyd, E.C. Dickey, H. Guo, J. Guo, A. Baker, S. Funihashi, C.A. Randall, J. Mater. Res. 32 (17) (2017) 3205, https://doi.org/10.1557/jmr.2017.262.
[10] D. Wang, H. Guo, C.S. Morandi, C.A. Randall, S. Trolier-McKinstry, APL Mater. 6 (2018) 1, https://doi.org/10.1063/1.5004420.
[11] S.S. Anandakrishnan, S. Yadav, M. Tabeshfar, V. Balanov, T. Kaushalya, M. Nelo, J. Peräntie, J. Juuti, Y. Bai, Glob. Challenges 7 (2023) 8, https://doi.org/10.1002/gch2.202300061.
[12] M. Das, R. Karthik, P.R. Sreeram, A. Jana, A. Dixit, S.K. Panda, D. Roy, C.S. Tiwary, A.C.S. Sustain, Chem. Eng. 11 (39) (2023) 14308, https://doi.org/10.1021/acssuschemeng.3c03873.
[13] A. Šutka, A. Šutka, H. Dundurs, B. del Rosal, M. Iesalnieks, K. Mālnieks, A. Linarts, A.J. Barlow, R.T. Leon, A.V. Ellis, P.C. Sherrell, Adv. Energy Sustain. Res. 5 (2024) 6, https://doi.org/10.1002/aesr.202300259.
[14] P.K. Annamalai, A.K. Nanjundan, D.P. Dubal, J.B. Baek, Adv. Mater. Technol. 6 (2021) 3, https://doi.org/10.1002/admt.202001164.
[15] B. Baytekin, H.T. Baytekin, B.A. Grzybowski, Energy Environ. Sci. 6 (2013) 3467, https://doi.org/10.1039/c3ee41360h.
[16] M.P. Silva, R.S. Martins, H. Carvalho, J.M. Nobrega, S. Lanceros-Mendez, Polym. Test. 32 (6) (2013) 1041, https://doi.org/10.1016/j.polymertesting.2013.05.010.
[17] M. Ismail, Z. Wu, L. Zhang, J. Ma, Y. Jia, Y. Hu, Y. Wang, Chemosphere 228 (2019) 212, https://doi.org/10.1016/j.chemosphere.2019.04.121.
[18] X. Xu, Y. Jia, L. Xiao, Z. Wu, Chemosphere 193 (2018) 1143, https://doi.org/10.1016/j.chemosphere.2017.11.116.
[19] H. Lei, H. Zhang, Y. Zou, X. Dong, Y. Jia, F. Wang, J. Alloys Compd. 809 (2019) 151840, https://doi.org/10.1016/j.jallcom.2019.151840.
[20] M. Yang, J. Liu, D. Liu, J. Jiao, N. Cui, S. Liu, Q. Xu, L. Gu, Y. Qin, Research 2021 (2021) 9793458, https://doi.org/10.34133/2021/9793458.
[21] S. Bhunia, S. Chandel, S.K. Karan, S. Dey, A. Tiwari, S. Das, N. Kumar, R. Chowdhury, S. Mondal, I. Ghosh, A. Mondal, B.B. Khatua, N. Ghosh, C. Malla Reddy, Science 373 (321) (2021) 6552, https://doi.org/10.1126/science.abg3886.
[22] M. Tabeshfar, M. Nelo, S.S. Anandakrishnan, M. Siddiqui, J. Peräntie, P. Tofel, H. Jantunen, J. Juuti, Y. Bai, Small Methods 8 (2023) 5, https://doi.org/10.1002/smtd.202300830.
[23] S.S. Anandakrishnan, M. Tabeshfar, M. Nelo, J. Peräntie, H. Jantunen, J. Juuti, Y. Bai, RSC Sustain. 2 (4) (2024) 961, https://doi.org/10.1039/d3su00348e.
[24] S. S. Anandakrishnan, M. Nelo, M. Tabeshfar, V. Kraft, N. H. Khansur, J. Peräntie, Y. Bai, Influence of permittivity between fillers and binders on properties of upside-

down composites for recycling purpose, Preprint 2025, URL: https://dx.doi.org/10.2139/ssrn.5188484.
[25] H. Khanbareh, S. Van Der Zwaag, W.A. Groen, AIP Conf. Proc. 1627 (1) (2014) 46, https://doi.org/10.1063/1.4901656.
[26] H. Khanbareh, S. Van Der Zwaag, W.A. Groen, Smart Mater. Struct. 23 (2014) 10, https://doi.org/10.1088/0964-1726/23/10/105030.
[27] P. Eltouby, I. Shyha, C. Li, J. Khaliq, Ceram. Int. 47 (13) (2021) 17813, https://doi.org/10.1016/j.ceramint.2021.03.126.
[28] J. Khaliq, D.B. Deutz, J.A.C. Frescas, P. Vollenberg, T. Hoeks, S. van der Zwaag, P. Groen, Ceram. Int. 43 (2) (2017) 2774, https://doi.org/10.1016/j.ceramint.2016.11.108.
[29] Y. Zhang, M. Xie, J. Roscow, Y. Bao, K. Zhou, D. Zhang, C.R. Bowen, J. Mater. Chem. A 5 (14) (2017) 6569, https://doi.org/10.1039/c7ta00967d.
[30] P. Kabakov, T. Kim, Z. Cheng, X. Jiang, S. Zhang, Annu. Rev. Mater. Res. 53 (2023) 165, https://doi.org/10.1146/annurev-matsci-080921-092839.
[31] K. Uchino, in Adv. Piezoelectric Mater. (Ed.: K. Uchino), Woodhead Publishing, 2010, pp. 318–346.
[32] D. Deutz, Flexible piezoelectric composites bridging the gap between, Mater. Appl. (2017), https://doi.org/10.4233/uuid:3ed1b44e-44f4-4b84-abd1-34722d106c22.
[33] M. De Jong, W. Chen, H. Geerlings, M. Asta, K.A. Persson, Sci. Data 2 (2015) 150053, https://doi.org/10.1038/sdata.2015.53.
[34] K.F. Garrity, Phys. Rev. B 97 (2018) 2, https://doi.org/10.1103/PhysRevB.97.024115.
[35] P. Baettig, N.A. Spaldin, Appl. Phys. Lett. 86 (2005) 1, https://doi.org/10.1063/1.1843290.
[36] T.E. Smidt, S.A. Mack, S.E. Reyes-Lillo, A. Jain, J.B. Neaton, Sci. Data 7 (2020) 72, https://doi.org/10.1038/s41597-020-0407-9.
[37] M.M. Rahman, S. Janwari, M. Choi, U.V. Waghmare, J. Lee, Mater. Des. 236 (2023) 112518, https://doi.org/10.1016/j.matdes.2023.112518.
[38] Q. Zhu, P. Xu, T. Lu, X. Ji, M. Shao, Z. Duan, W. Lu, Mater. Des. 238 (2024) 112642, https://doi.org/10.1016/j.matdes.2024.112642.
[39] P.V. Balachandran, B. Kowalski, A. Sehirlioglu, T. Lookman, Nat. Commun. 9 (2018) 1668, https://doi.org/10.1038/s41467-018-03821-9.
[40] H.R.O. Rocha, R. Roukos, S. Abou Dargham, J. Romanos, D. Chaumont, J.A. L. Silva, H. Wörtche, Mater. Des. 243 (2024) 113053, https://doi.org/10.1016/j.matdes.2024.113053.
[41] F. Ricci, S.E. Reyes-Lillo, S.A. Mack, J.B. Neaton, NPJ Comput. Mater. 10 (2024) 15, https://doi.org/10.1038/s41524-023-01193-3.
[42] W. Li, T. Yang, C. Liu, Y. Huang, C. Chen, H. Pan, G. Xie, H. Tai, Y. Jiang, Y. Wu, Z. Kang, L.Q. Chen, Y. Su, Z. Hong, Adv. Sci. 9 (2022) 13, https://doi.org/10.1002/advs.202105550.
[43] Z.H. Shen, J.J. Wang, J.Y. Jiang, S.X. Huang, Y.H. Lin, C.W. Nan, L.Q. Chen, Y. Shen, Nat. Commun. 2019 (1843) 10, https://doi.org/10.1038/s41467-019-09874-8.
[44] Z.H. Shen, Z.W. Bao, X.X. Cheng, B.W. Li, H.X. Liu, Y. Shen, L.Q. Chen, X.G. Li, C. W. Nan, NPJ Comput. Mater. 7 (2021) 110, https://doi.org/10.1038/s41524-021-00578-6.
[45] Z.H. Shen, J.J. Wang, Y. Lin, C.W. Nan, L.Q. Chen, Y. Shen, Adv. Mater. 30 (2018) 2, https://doi.org/10.1002/adma.201704380.
[46] K. Singh, J. Adhikari, J. Roscow, Mater. Today Commun. 38 (2024) 108288, https://doi.org/10.1016/j.mtcomm.2024.108288.
[47] J. Chen, C. Ayranci, T. Tang, Mater. Today Chem. 30 (2023) 101571, https://doi.org/10.1016/j.mtchem.2023.101571.
[48] Z.M. Tsikriteas, J.I. Roscow, C.R. Bowen, H. Khanbareh, Adv. Eng. Mater. 25 (2023) 22, https://doi.org/10.1002/adem.202301269.
[49] A. Samanta, S. Yadav, Z. Gu, C.J.G. Meyers, L. Wu, D. Chen, S. Pandya, R.A. York, L.W. Martin, J.E. Spanier, I. Grinberg, Adv. Mater. 34 (2022) 7, https://doi.org/10.1002/adma.202106021.
[50] S. Yadav, A. Samanta, O. Shafir, I. Grinberg, Adv. Mater. 34 (2022) 7, https://doi.org/10.1002/adma.202106105.
[51] S.S. Anandakrishnan, Y. Bai, Dataset of a statistical study on factors influencing piezoelectric properties of upside-down composites towards machine learning-driven development for recycling, Fairdata.fi Etsin (2024), https://doi.org/10.23729/fd-4296899f-a945-3eb1-9a77-49baa24744af.
[52] D.A. Van Den Ende, B.F. Bory, W.A. Groen, S. Van Der Zwaag, J. Appl. Phys. 107 (2010) 2, https://doi.org/10.1063/1.3291131.
[53] C.R. Bowen, A. Perry, A.C.F. Lewis, H. Kara, J. Eur. Ceram. Soc. 24 (2) (2004) 541, https://doi.org/10.1016/S0955-2219(03)00194-8.
[54] M. Nelo, T. Siponkoski, H. Kähäri, K. Kordas, J. Juuti, H. Jantunen, J. Eur. Ceram. Soc. 39 (11) (2019) 3301, https://doi.org/10.1016/j.jeurceramsoc.2019.04.052.
[55] M. Nelo, J. Peräntie, T. Siponkoski, J. Juuti, H. Jantunen, Appl. Mater. Today 15 (2019) 83, https://doi.org/10.1016/j.apmt.2018.12.021.
[56] T. Siponkoski, M. Nelo, N. Ilonen, J. Juuti, H. Jantunen, Compos. Part B Eng. 229 (2022) 109486, https://doi.org/10.1016/j.compositesb.2021.109486.
[57] N. Kuzmić, S.D. Škapin, M. Nelo, H. Jantunen, M. Spreitzer, Front. Mater. 8 (2021) 669421, https://doi.org/10.3389/fmats.2021.669421.
[58] H. Khanbareh, S. van der Zwaag, W.A. Groen, J. Intell. Mater. Syst. Struct. 28 (18) (2017) 2467, https://doi.org/10.1177/1045389X17689928.
[59] V.L. Stuber, D.B. Deutz, J. Bennett, D. Cannel, D.M. de Leeuw, S. van der Zwaag, P. Groen, Energy Technol. 7 (1) (2019) 177, https://doi.org/10.1002/ente.201800419.
[60] Y. Zhang, M. Xie, J. Roscow, C. Bowen, Mater. Res. Bull. 112 (2019) 426, https://doi.org/10.1016/j.materresbull.2018.08.031.
[61] A.A. Tezcan, C.R. Bowen, G. Poulin-Vittrant, H. Khanbareh, J.I. Roscow, IEEE Int. Symp. Appl. Ferroelectr., IEEE (2023) 7, https://doi.org/10.1109/ISAF53668.2023.10265622.
[62] M. Yan, J. Zhong, S. Liu, Z. Xiao, X. Yuan, D. Zhai, K. Zhou, Z. Li, D. Zhang, C. Bowen, Y. Zhang, Nano Energy 88 (2021) 106278, https://doi.org/10.1016/j.nanoen.2021.106278.
[63] R. Guo, J.I. Roscow, C.R. Bowen, H. Luo, Y. Huang, Y. Ma, K. Zhou, D. Zhang, J. Mater. Chem. A 8 (6) (2020) 3135, https://doi.org/10.1039/c9ta11360f.
[64] J. Guo, S.S. Berbano, H. Guo, A.L. Baker, M.T. Lanagan, C.A. Randall, Adv. Funct. Mater. 26 (39) (2016) 7115, https://doi.org/10.1002/adfm.201602489.
[65] Ferroperm Piezoceramics, "Soft PZT Type PZ29 data sheet," 2018, URL https://www.ferropermpiezoceramics.com/wp-content/uploads/2021/10/Datasheet-soft-pz29.pdf.
[66] Americanpiezo International Ltd., "Physical and Piezoelectric Properties of APC Materials," 2020, URL https://www.americanpiezo.com/apc-materials/piezoelectric-properties.html.
[67] F. Li, S. Zhang, D. Damjanovic, L.Q. Chen, T.R. Shrout, Adv. Funct. Mater. 28 (2018) 37, https://doi.org/10.1002/adfm.201801504.
[68] S. Banerjee, K.A. Cook-Chennault, Compos. Part A 43 (9) (2012) 1612, https://doi.org/10.1016/j.compositesa.2012.03.014.
[69] A. Guevara-Morales, A.C. Taylor, J. Mater. Sci. 49 (2014) 1574, https://doi.org/10.1007/s10853-013-7840-5.
[70] Epo-Tek, "Epo-tek ® med-301," 2018, URL https://www.epotek.com/docs/en/Datasheet/MED-301.pdf.
[71] R.N. Palchesko, L. Zhang, Y. Sun, A.W. Feinberg, PLoS One 7 (12) (2012) e51499, https://doi.org/10.1371/journal.pone.0051499.
[72] M. Tabeshfar, M. Nelo, S. S. Anandakrishnan, J. Peräntie, Y. Bai, Study on recycling of lead-based piezoceramics using upside-down compositing method and trimethylchloromethyl ammonium-based halide perovskite binder, Preprint 2025, URL: https://dx.doi.org/10.2139/ssrn.5190197.
[73] N. Kuzmić, S.D. Škapin, M. Nelo, H. Jantunen, M. Spreitzer, Open Ceram. 16 (2023) 100495, https://doi.org/10.1016/j.oceram.2023.100495.
[74] M. Baek, F. DiMaio, I. Anishchenko, J. Dauparas, S. Ovchinnikov, G.R. Lee, J. Wang, Q. Cong, L.N. Kinch, R. Dustin Schaeffer, C. Millán, H. Park, C. Adams, C. R. Glassman, A. DeGiovanni, J.H. Pereira, A.V. Rodrigues, A.A. Van Dijk, A. C. Ebrecht, D.J. Opperman, T. Sagmeister, C. Buhlheller, T. Pavkov-Keller, M. K. Rathinaswamy, U. Dalwadi, C.K. Yip, J.E. Burke, K. Christopher Garcia, N. V. Grishin, P.D. Adams, R.J. Read, D. Baker, Science 373 (871) (2021) 6557, https://doi.org/10.1126/science.abj8754.
[75] A.V. Goncharenko, V.Z. Lozovski, E.F. Venger, Opt. Commun. 174 (1–4) (2000) 19, https://doi.org/10.1016/S0030-4018(99)00695-1.
[76] A. Tuluk, T. Mahon, S. van der Zwaag, P. Groen, J. Alloys Compd. 868 (2021) 159186, https://doi.org/10.1016/j.jallcom.2021.159186.
[77] Z.M. Tsikriteas, R.A. Heylen, S. Jindal, E. Mancuso, Z. Li, H. Khanbareh, Adv. Mater. Technol. 8 (7) (2023) 2202127, https://doi.org/10.1002/admt.202202127.
[78] T. Yamada, T. Ueda, T. Kitayama, J. Appl. Phys. 53 (6) (1982) 4328, https://doi.org/10.1063/1.331211.
[79] N. Kuzmić, E. Terbovšek, S.D. Škapin, M. Nelo, H. Jantunen, M. Spreitzer, Ceram. Int. 50 (18) (2024) 33180, https://doi.org/10.1016/j.ceramint.2024.06.129.
[80] A. Jabr, N. Kuzmić, S.D. Škapin, H. Jantunen, M. Nelo, M. Spreitzer, R. Bermejo, J. Eur. Ceram. Soc. 44 (15) (2024) 116782, https://doi.org/10.1016/j.jeurceramsoc.2024.116782.
[81] V.L. Stuber, T.R. Mahon, S. Van Der Zwaag, P. Groen, Mater. Res. Express 7 (1) (2019) 015703, https://doi.org/10.1088/2053-1591/ab5bb3.
[82] J. Roscow, Y. Zhang, J. Taylor, C.R. Bowen, Eur. Phys. J. Spec. Top. 224 (2015) 2949, https://doi.org/10.1140/epjst/e2015-02600-y.
[83] T. Siponkoski, M. Nelo, J. Palosaari, J. Peräntie, M. Sobocinski, J. Juuti, H. Jantunen, Compos. Part B Eng. 80 (2015) 217, https://doi.org/10.1016/j.compositesb.2015.05.018.
[84] M. Väätäjä, H. Kähäri, K. Ohenoja, M. Sobocinski, J. Juuti, H. Jantunen, Sci. Rep. 8 (2018) 15955, https://doi.org/10.1038/s41598-018-34408-5.
[85] L. Zhao, Y. Zhang, M. Yan, J. Li, X. Xiong, J. Roscow, D. Zhang, C. Bowen, J. Eur. Ceram. Soc. 45 (2025) 116934, https://doi.org/10.1016/j.jeurceramsoc.2024.116934.
[86] S. Ghosh, S.D.P. Tarafder, Sci. Rep. 15 (2025) 6631, https://doi.org/10.1038/s41598-025-91196-5.
[87] Q. Chen, C. Xiao, Z. Yang, J. Tabet, X. Chen, Compos. Part A-Appl. S. 186 (2024) 108421, https://doi.org/10.1016/j.compositesa.2024.108421.
[88] J. Hu, Y. Song, Chem. Phys. Lett. 791 (2022) 139359, https://doi.org/10.1016/j.cplett.2022.139359.
[89] L. Ni, J. Chen, G. Chen, D. Zhao, G. Wang, S.S. Aphale, Eng. Appl. Artif. Intel. 136 (2024) 108904, https://doi.org/10.1016/j.engappai.2024.108904.